Numerical simulation and experimental research of the integrated high-power LED radiator

J H Xiang[1], C L Zhang, Z J Gan, C Zhou, C G Chen and S Chen

School of Mechanical and Electric Engineering, Guangzhou University, Guangzhou 510006, China

Email: xiangjh@gzhu.edu.cn

Abstract. The thermal management has become an urgent problem to be solved with the increasing power and the improving integration of the LED (light emitting diode) chip. In order to eliminate the contact resistance of the radiator, this paper presented an integrated high-power LED radiator based on phase-change heat transfer, which realized the seamless connection between the vapor chamber and the cooling fins. The radiator was optimized by combining the numerical simulation and the experimental research. The effects of the chamber diameter and the parameters of fin on the heat dissipation performance were analyzed. The numerical simulation results were compared with the measured values by experiment. The results showed that the fin thickness, the fin number, the fin height and the chamber diameter were the factors which affected the performance of radiator from primary to secondary.

Keywords: High-power LED radiator, Optimization, Experiment, Phase-change heat transfer.

1. Introduction

The thermal management issues, which hindered the further development of high-power LED, have increasingly attracted attention with the development of the high-power LED to the high integration and power. The heat flux density of high-power LED chips had reached as high as 200 W/cm^2 [1]. Poor heat dissipation leads to over-high temperatures of LED chips, which result in reduction of LED performances, or even burning down. The cooling of traditional high-power LED systems generally use solid radiators made of aluminum, copper or composite materials. Their large thermal diffusion leads to inefficient cooling, and has been difficult to meet the cooling demands of the LED with increasing power. On the other hand, the performance of phase-change heat transfer can be enhanced more than 10 times compared to conventional metal heat transfer [2], which has been widely applied in the heat dissipation in the fields of microelectronics and optoelectronics.

The application of solid aluminum radiators and phase-change heat transfer technology in the cooling of high-power LED systems has attracted many researchers' attention [3-4]. Compared with the phase-change radiators, the solid aluminum radiators have lower heat transfer power and larger thermal resistance, which are only suitable for low-power LED lights. However, the use of phase-change heat transfer technology becomes a trend in the high-power LED system cooling with the increase of the LED power [2]. Bladimir et al. [5] had simulated the cooling effects of a micro-jet and a micro-channel water-cooled plate on the LED using a 3D model, and calculated the thermal resistance of the influent with different flow rates. The results showed that the thermal resistance of the micro-channel water-cooled plate was lower than the micro-jet thermal resistance. Wang [6] established a radiator model of a LED spotlight in natural convection condition. By changing the fin spacing, the fin thickness and the LED substrate material, numerical simulations were performed with various placing angles. Cheng et al. [7] analyzed the integral multi-fin radiators on the PCB substrate under forced convection conditions using finite element analysis. The results showed that the junction temperature of the 1W LED arrays reached 123℃ without fan and fins, while the junction temperature decreased to 82℃ with forced convection cooling.

In this study, phase-change heat transfer and fin heat dissipation were combined in a radiator structure. In the phase-change chamber, the endothermic and exothermic processes of the working fluid during the cycle of vaporization-condensation realized efficient heat transfer, which result in an isothermal condition between the external fins at the top and the bottom of the radiator. With a certain heating power, the effects of the chamber diameter, the fin number, height and thickness on the heat transfer performance of the radiators were studied. The radiator was optimized using the approach combining the orthogonal tests and the numerical simulations, and the results were compared with the actual experiments.

2. Working principle and numerical modeling of the phase-change radiators

2.1. Working principle of the radiator

The working principle of the radiators is shown in Figure 1. The radiator is divided into two parts: the center section of the enhanced heat transfer and the periphery section of the cooling. When the LED heat the bottom of radiator, the working fluid (acetone) in the boiling structure is heated and evaporated. The steam rapidly flows and fills the whole chamber. When the steam contacts the condensing end, it rapidly condenses and releases the latent heat. Then, the condensed working fluid returns to the evaporation surface under the action of gravity. With this type of cycle, the heat continuously transfers from the evaporation surface to the condensation surface, and then dissipates into the atmosphere through the cooling fins. This structure can eliminate the contact resistance due to the seamless connection between the center section of the enhanced heat transfer and the surrounding section of the cooling.

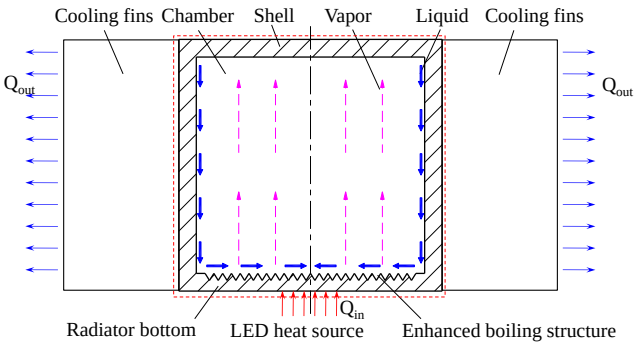

Figure 1. Working principle of the radiator.

2.2. Numerical modeling of the radiator cooling fins

According to the LED working requirements and the thermal design theory, the radiator was simplified before the simulations. The LED heat sources were simplified to the same geometric shape. The thermal resistance of the boiling structure was simplified as the thermal contact resistance between the hot end of the radiator and the phase-change chamber. The phase-change cavity was simplified as a solid cylinder with high thermal conductivity, and its axial heat transfer performance was evaluated as an equivalent thermal conductivity Y [8]:

$$Y = \frac{Q_{\text{in}}\, C}{(T_{\text{Z}} - T_{\text{L}})M} \tag{1}$$

where, Q_{in}-the heat source power, C-the effective length of the heat transfer, M-the sectional area, T_Z-the average temperature at the evaporating end, T_L-the average temperature at the condensation end.

The thermal conductivity of the phase-change cavity behaved as isotropic (Eq. 1). The temperature evaluation points in the cooling system located at the heat source, the hot end and the cold end of the phase-change cavity. After the property definition of the model, the setting of the initial and boundary conditions, the mesh generation and the solving, the average temperatures at the heat source and each evaluation point were exported.

Table 1. Factors and levels of orthogonal test.

Factors	Chamber diameter /A	Fin height /B (mm)	Fin thickness /C (mm)	Fin number /D (piece)
1#	55	160	3(4)	36
2#	65	155	2.5(3.5)	32
3#	70	145	1.5(2.5)	40
4#	60	150	2(3)	28

In order to improve the heat transfer performance of the radiator, the geometric parameters including the height, the thickness, the number, and the length of the fins in the phase-change radiator were optimized. The thicknesses of the inner and outer layer of the fin were represented as c(d). The test was four factors and four levels, and the interactions between factors were ignored. Factors and levels of orthogonal test are shown in Table 1. In order to facilitate the later analysis of variance, the orthogonal table with $L_{16}(4^5)$ type was selected. The model of the phase-change radiator is shown in

Figure 2.

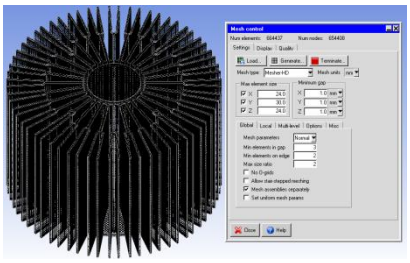

(a) Numerical model

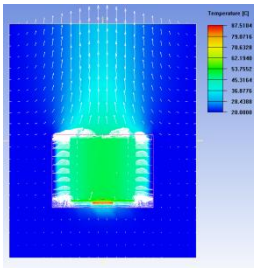

(b) slice image of the temperature and the airflow velocity

Figure 2. The numerical model and the temperature distribution of the radiator.

The calculation equation of the comprehensive index *X*, which take an overall evaluation of the results, is shown in Eq. 2.

$$X=\alpha_1 T_{hs}+\alpha_2 T_{ah}+\alpha_3(T_{hs}-T_{ah}) \quad (2)$$

where, T_{hs}-the central temperature in the heat source, T_{ah}-the average temperature of the heat source, α_1, α_2, and α_3 the proportion coefficients of the index significances. Comprehensively considering all factors, the values of α_1, α_2, and α_3 in this test were selected as 0.4, 0.3 and 0.3, respectively.

In the tests, the third column was randomly selected as the blank column, and the levels of each factor were filled in the orthogonal table. With temperature of 20°C, 16 models with various parameters were numerically simulated. The highest temperature and the average temperature of the heat source for each model were obtained, and the comprehensive index *X* was calculated.

3. Results and analysis

3.1. Intuitive analysis

In the intuitive analysis, the larger the range *R* is the greater the effect of the factor in this column on the index. Within the selected range of the level values, the significance sequence is C (fin thickness), D (fin number), B (fin height) and A (chamber diameter) from primary to secondary due to $R_C>R_D>R_B>R_A$. In the tests, the test index is corresponding to the cooling performance of the radiator. The cooling performance is reflected by the temperature level, therefore, it is better to have a smaller *X* value. The significance sequence of the factors on the index were both C, D, B, and A from primary to secondary form the variance analysis. The simulation parameters and the simulation results for the optimized scheme are showed in Table 2.

Table 2. The simulation results of optimized scheme.

A (mm)	B (mm)	C (mm)	D (piece)	T_{hs} (℃)	T_{ah} (℃)	X
60	155	1.5(2.5)	32	87.51	80.01	61.25

3.2. The influence of radiator height on the performance

To ensure junction temperature of chip $T_j \leqq 85$°C, the verified heights were 55mm, 75mm, 95mm and 115mm in the orthogonal tests. Numerical simulations were conducted with various powers for the

above verified heights. The values obtained from the simulations are shown in Figure 3.

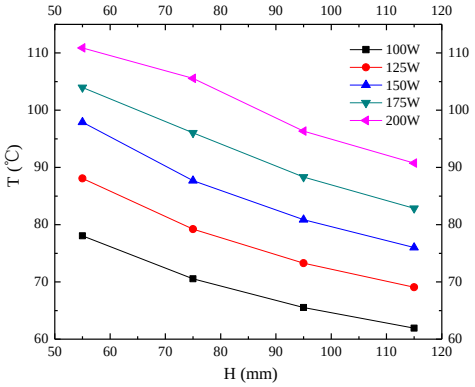

Figure 3. Simulated temperatures with various fin heights.

As can be seen from Figure 3, the height increase led to the temperature decrease with the same power, while the power increase resulted in the temperature increase with the same height. Regarding the cost reduction, the height value should be selected as low as possible in the test range with the premise of satisfying the cooling performance. Therefore, it was more appropriate to select a radiator height of 55, 75, 95 and 115 mm with a heating power of 100, 125, 150 and 200W, respectively.

3.3. Comparison between the experimental and the simulation results

With an ambient temperature of 20°C and heating powers of 50,100,125,150,175 and 200 W, the measured temperatures by thermocouples compared with the simulated temperatures at the corresponding points are shown in Figure 4.

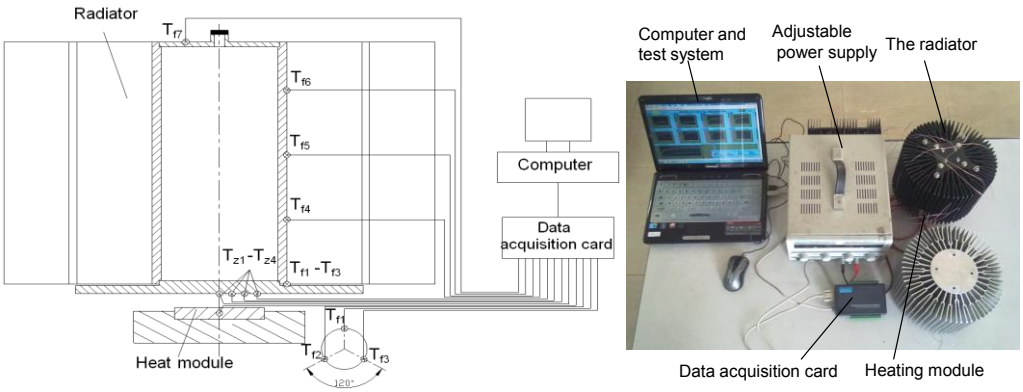

(a) Schematic diagram of thermocouple distribution (b) Testing process

Figure 4. Temperature testing system.

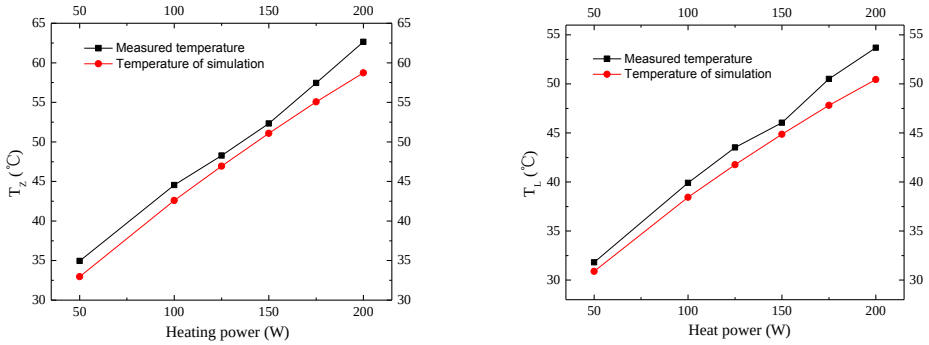

(a) Average temperature at the evaporating end (b) Average temperature at the condensation end

Figure 5. Comparison between the measured temperatures and the simulated temperatures.

From Figure 5, the trends of the measured temperatures and the simulated temperatures were consistent at the corresponding positions. The maximum error between the simulated and the measured temperature was 6°C. The relative errors were below 5% for most data, and were less than 10% for all the data. This was because the radiator model was simplified. Removing subtle geometric characteristics had some effect on the heat transfer process.

4. Conclusions

(1) The employment of the phase-change heat transfer technique led to an isothermal condition of the radiator fins. The radiator was optimized by using a combination of orthogonal tests and numerical simulations, resulting an improvement of the cooling efficiency.

(2) The significance sequence was the fin thickness, the fin number, the fin height and the chamber diameter from primary to secondary. The trend of the measured temperatures was consistent with the simulated temperatures at corresponding positions.

(3) With a certain heating power, the heat source temperature decreased with the increase of the radiator height. With a heating power of 100,125,150 and 200W, it was more appropriate to select a radiator height of 55, 75, 95 and 115mm, respectively.

Acknowledgements

This research were supported by the National Nature Science Foundation of China (51575115, 51275099); the project of Guangdong research program (Yq2013127, 2014A010105053); Project (201510010069) supported by Guangzhou research program; Guangzhou Key Laboratory for Monitoring and Control of Electromechanical Equipment (2060402).

References

[1] Wan Z M, Chen M, Liu W and Liu J 2010 Research on porous micro heat sink for thermal management of high power LED *Journal of Mechanical Engineering* **46**(8) 109-113
[2] Vasiliev L L 2008 Micro and miniature heat pipes-electronic component coolers *Applied Thermal Engineering* **28**(4) 266-273
[3] Kim L, Jong H C and Sun H J *et al* 2007 Thermal analysis of LED array system with heat pipe *Thermochimica Acta* **455**(1-2) 21-25
[4] Liu S, Yang J and Gan Z *et al* 2008 Structural optimization of a microjet based cooling system for high power LEDs *International Journal of Thermal Sciences* **47**(8) 1086-1095
[5] Bladimir R A, Feng B and Peterson G P 2013 Comparison and optimization of single-phase

liquid cooling devices for the heat dissipation of high-power LED arrays *Applied Thermal Engineering* **59**(1-2) 648-659
[6] Wang J C 2014 Thermal module design and analysis of a 230 W LED illumination lamp under three incline angles *Microelectronics Journal* **45**(4) 416-423
[7] Cheng H H, Huang D S and Lin M T 2012 Heat dissipation design and analysis of high power LED array using the finite element method *Microelectronics Reliability* **52**(5) 905-911
[8] Zhan D D and Qian J Y 2012 Study on effective conductivity of heat pipe embedded al plates *Electro-Mechanical Engineering* **04** 12-14